The role of MOFs in Thin-Film Nanocomposite (TFN) membranes

The role of MOFs in Thin-Film Nanocomposite (TFN) membranes

Cédric Van Goethem,[a] Rhea Verbeke,[a] Martin Pfanmöller,[b,c] Tönjes Koschine,[a] Marcel Dickmann[d], Tanja Timpel-Lindner[e], Werner Egger[f], Sara Bals,[b] Ivo F.J. Vankelecom[a,]*

[a] Center for Surface Chemistry and Catalysis, Faculty of Bioscience Engineering Sciences, KU Leuven, Celestijnenlaan 200F PO Box 2461, 3001 Leuven, Belgium

[b] Electron Microscopy for Material Science (EMAT), Department of Physics, University of Antwerp, Groenenborgerlaan 171, Antwerp 2020 Belgium, Belgium

[c] Centre for Advanced Materials, Heidelberg University, 69120 Heidelberg, Germany

[d] FRM II, Technische Universität München, Lichtenbergstraße 1, 85748 Garching, Germany

[e] Institut für Physik, Universität der Bundeswehr München, Werner-Heisenberg-Weg 39, 85577 Neubiberg, Germany

[f] Institut für Angewandte Physik und Messtechnik, Universität der Bundeswehr München, Werner-Heisenberg-Weg 39, 85579 Neubiberg, Germany

Corresponding author

* ivo.vankelecom@kuleuven.be

ABSTRACT

Incorporation of MOFs in interfacially polymerized Thin-Film Nanocomposite (TFN) membranes has widely been shown to result in increased membrane performance. However, the exact functioning of these membranes is poorly understood as large variability in permeance increase, filler incorporation and rejection changes can be observed in literature. The synthesis and functioning of TFN membranes (herein exemplified by ZIF-8 filled polyamide (PA) membranes prepared via the EFP method) was investigated via targeted membrane synthesis and thorough characterization via STEM-EDX, XRD and PALS. It is hypothesized that the acid generated during the interfacial polymerization (IP) at least partially degrades the crystalline, acid-sensitive ZIF-8 and that this influences the membrane formation (through so-called secondary effects, i.e. not strictly linked to the pore morphology of the MOF). Nanoscale HAADF-STEM imaging and STEM-EDX Zn-mapping revealed no ZIF-8 particles but rather the presence of randomly shaped regions with elevated Zn-content. Also XRD failed to show the presence of crystalline areas in the composite PA films. As the addition of the acid-quenching TEA led to an increase in the diffraction signal observed in XRD, the role of the acid was confirmed. The separate addition of dissolved Zn^{2+} to the synthesis of regular TFC membranes showed an increase in permeance while losing some salt retention, similar to observations regularly made for TFN membranes. While the addition of a porous material to a TFC membrane is a straightforward concept, all obtained results indicate that the synthesis and performance of such composite membranes is often more complex than commonly accepted.

KEYWORDS: Thin-Film Nanocomposite (TFN) membrane; Metal-Organic Frameworks (MOFs); Interfacial Polymerization; Nanofiltration; Characterization

1.INTRODUCTION

Membrane-based water separations offer a green, easily scalable and efficient alternative to conventional water purification technologies. Pressure driven reverse osmosis (RO) and nanofiltration (NF) processes using thin-film composite (TFC) membranes are most frequently used for membrane-based water purification.[1] Also in the chemical industry, a continuous search exists for more energy- (and thus cost-) efficient separation technologies. The recovery of catalysts or pharmaceuticals from their reaction mixtures are only some examples that can be achieved through NF.[1–3]

TFC membranes are asymmetric composite membranes that combine the high flux and rejection of a very thin, yet dense (often polyamide (PA)) toplayer, with the mechanical strength of a support layer that is usually formed via phase inversion on a non-woven fabric substrate. Various methods exist for the preparation of composite membranes, but interfacial polymerization (IP) is most widely used. IP involves the use of two immiscible solvent phases each containing one monomer. Often a diamine (e.g. m-phenylenediamine) is dissolved in an aqueous phase and an acyl chloride (e.g. trimesoylchloride) is dissolved in an organic phase (e.g. hexane, isopar, …). Upon contact between the two phases, the diamine diffuses to the organic phase and reacts with the acyl chloride through a nucleophilic substitution to form a PA.[4]

Further improvement of the membrane performance is a necessity to further increase the efficiency and application range of membrane-based separations. Specifically for TFC membranes, various strategies are being investigated. Replacing the organic phase by ionic liquids, the introduction of sacrificial layers to achieve tight control over the IP and hence to reduce toplayer thickness, or the use of highly contorted and stiff monomers to

increase the free volume in the toplayer are only some of the strategies that have recently been investigated.[5–7] Another highly promising strategy is the incorporation of inorganic nanoparticles in the thin toplayer to form so-called thin-film nanocomposite (TFN) membranes.[8] The improved membrane permeance can have multiple origins. (i) Typically, when using porous fillers, the 'incorporated porosity' provides additional pathways for low-resistant solvent transport, (ii) interfacial voids between the filler and the PA, (iii) changes in membrane hydrophilicity and (iv) changes in the membrane structure (degree of cross-linking etc.). A wide range of fillers has been explored in TFN membranes, such as mesoporous silica, zeolites, multiwall carbon nanotubes (MWCNT's) and, metal-organic frameworks (MOFs), … .[9] The latter in particular have recently attracted a lot of interest as filler material in TFN membranes.[10–14]

MOFs are crystalline porous frameworks constructed from metal ions/clusters and organic linkers.[15] A vast amount of different framework topologies, chemistries and potential applications have been reported. The number of MOFs used as filler in TFN membranes is rapidly expanding since the first report of Sorribas et al. because these different MOF topologies and chemistries are expected to result in toplayers with different properties. The MOFs explored to date include ZIF-8,[10–14] ZIF-11,[16] MIL-53,[11] MIL-68,[16] MIL-101,[11,16] UiO-66[17] as well as modified/composite MOFs.[18,19] In addition to this, also the method to optimize the incorporation and effect of the MOF fillers received a lot of attention. Apart from the traditional MOF dispersion in the TMC phase, also dispersion in the aqueous phase,[14] layer-by-layer,[13] Langmuir-Schaefer,[20] dip-coating[21] and evaporation controlled positioning[10] techniques are being investigated.

Sorribas et al. (2014) used the MOFs ZIF-8, MIL-53, MIL-53-NH2 and MIL-101 as filler in TFN membranes.[11] All but the MIL-101 based TFN membrane, showed a relatively modest permeance increase (<40%) without rejection loss. The MIL-101-based TFN membrane showed a 110% permeance increase but did lose rejection. Duan et al. (2015) showed that an increased ZIF-8 concentration in the organic phase of up to 0.4 wt% realized a 160% permeance increase without salt rejection loss.[12] Wang et al. (2015) further investigated the influence of the phase in which to disperse the ZIF-8 nanoparticles and also the potential of a layer-by-layer approach for the preparation of ZIF-8 based TFN membranes. For both approaches however, an increase in salt passage was observed.[13,14] We recently developed 'Evaporation controlled Filler Positioning' (EFP) as a novel technique aimed at increasing the filler content in the toplayer. Very high permeance increases (>160%) were observed without compromising salt rejection.[10]

The continuously pushed boundaries of nanoscale characterization techniques through instrument and method research have already helped substantially to better understand the formation and structure of TFC membranes. Scanning Transmission X-ray Microscopy (STXM) characterization of a commercial TFC membrane allowed the identification of an unexpected polyMPD phase in the m-phenylenediamine (MPD) / trimesoyl chloride (TMC) based membrane toplayer.[22] Pacheco et al. (2010) reported two novel characterization approaches using conventional Transmission Electron Microscopy (TEM). A technique for cross-section imaging of isolated PA-films was developed as well as the projected area (PA) topview technique, which reveals thickness, morphology and mass-density of the PA toplayer.[23] Electron-tomography was very recently also applied for the 3D-characterization of PA TFC membrane samples, allowing

the visualization of the internal nanostructure of the PA toplayer.[24] 3D membrane imaging was also further demonstrated using Focussed Ion Beam – Scanning Electron Microscopy (FIB-SEM) achieving a resolution close to low-magnification TEM images. The resulting 3D-reconstruction provides a better picture of the toplayer morphology compared to the traditionally used AFM because of its ability to recognize 'overhanging features'.[25] The combination of nanoscale visualization and spectroscopic analysis via Energy Dispersive X-ray spectroscopy (EDX) and Electron Energy Loss Spectroscopy (EELS) in state-of-the-art Scanning Transmission Electron Microscopy (STEM), makes STEM one of the most potent characterization techniques for complex nanomaterials, such as TFN membranes.[26]

Literature investigation of the effects of MOF incorporation in TFN membranes reveals important inconsistencies in the relation between the membrane performance and structure change on one hand, and MOF type, concentration used during membrane synthesis and incorporation degree on the other hand. It is therefore hypothesized in the present work that the changed membrane performance is not only due to primary effects of the fillers (see above) but also to indirect, so-called secondary effects. These include (i) influence on the monomer transport across the interface, (ii) catalytic effects on the IP, (iii) catalytic effects on the hydrolysis of the acid chloride monomer and (iv) proton quenching capacity. The potential influence of these effects will be investigated in this manuscript using detailed characterization (STEM, PLEPS and XRD), in combination with targeted reference membrane synthesis and testing.

2. MATERIALS AND METHODS

2.1 Materials

$Zn(NO_3)_2.6H_2O$ (>99%) and 2-methylimidazole (HMim , 99%) were obtained from Sigma Aldrich. N-methylpyrrolidone (NMP, 99%), trimesoyl chloride (TMC, 98%) and m-phenylene diamine (MPD, >99%) were obtained from Acros Organics. Polysulfone (PSf, Udel P-1700) was obtained from Solvay, ethanol (EtOH, absolute grade) from Fischer chemical and sodium chloride was obtained from VWR (AnalaR Normapur). All chemical were used without further purification. Polyethylene/polypropylene (PE/PP) non-woven support was obtained from Freudenberg (Novatex 2471).

2.2 Support preparation

Supports for all TFC-membranes were prepared according to Hermans et al. (2015).[4] An 18 wt% solution of PSf (dried at 100°C) in NMP was prepared. The solution was stirred for at least 12 h and left to degas for another 12h before casting. A 200 µm thick layer of the polymer solution was cast on the non-woven (impregnated with NMP to prevent intrusion) using a Braive Instruments automated coater at a speed of 0.077 m/s in a temperature and humidity controlled room (20 ± 2 °C, 20-40% RI). The membrane was immediately transferred to the coagulation bath containing deionised water. Membranes were stored until further use in a beaker containing deionized water. A representative SEM cross-section image of the support membrane showing its macrovoid structure can be seen in Figure S1.

2.3 ZIF-8 synthesis

ZIF-8 particles were synthesized solvothermally according to Wee et al.[27] 11.75 g of $Zn(NO_3).6H_2O$ and 25.92 g of HMim were separately dissolved in 200 ml DMF each. The HMim solution was added to the Zn^{2+} solution under vigorous stirring for 5 minutes. The mixture was transferred to a Scott bottle and put in the oven for 4 h at 413 K. The mixture was allowed to cool down to room temperature after which the particles were collected via centrifugation and washed 3 times with methanol. Transfer of the particles from methanol to hexane for the experiments was performed through solvent exchange (3x) through centrifugation. ZIF-8 concentrations were determined through measuring the weight of ZIF-8 remaining after evaporation of the solvent from a 5 ml sample taken from a homogeneous dispersion. A representative TEM image of the nanoparticles can be seen in Figure S2.

2.4 Synthesis EFP-TFN membranes

EFP-TFN membranes were synthesized as reported by Van Goethem et al. (2016). The supports were impregnated with a 2 wt% aqueous solution of MPD for at least 10 min. Excess solution was removed using a rubbery wiper before covering the supports with 12.5 ml of a ZIF-8 dispersion in hexane. The ZIF-8 concentration was varied between 0.0025 and 0.4 w/v%, but the 0.005 and 0.1 w/v% based membranes were further investigated in this research The hexane was then allowed to evaporate under atmospheric conditions. To form the composite toplayer, the membrane was subsequently covered with 12.5 ml of 0.1 wt% TMC in hexane for 1 min. The TMC-solution was then drained off and the membrane surface was washed with fresh hexane and

allowed to dry for 1 min. The resulting TFN-membranes were stored in deionized water until further use.

2.5 Synthesis Zn-Mim TFC membranes

Zn / Mim TFC-membranes were synthesized similar to conventional TFC-membranes. Zn(NO3).6H2O or HMim was dissolved in MilliQ deionized water (R > 18.2 MΩ.cm) together with MPD (2 wt%). The supports were impregnated in this solution for at least 10 min. Excess solution was removed using a rubbery wiper before covering the membranes (10 cm^2) with 12.5 ml of a 0.1 wt% TMC in hexane solution. After 1 min, the TMC-solution was drained off and the membrane surface was rinsed with fresh hexane. The resulting TFC- membranes were stored in deionized water until further use.

2.6 Ex-situ free standing nanocomposite PA film synthesis

Powderized free-standing nanocomposite PA films were prepared for XRD analysis. To obtain sufficient material, a large syringe (diameter 2.5 cm) with sealed nozzle was first filled with the aqueous MPD solution (2 wt%). Thereafter, the ZIF-8 (0.2 wt%) dispersion in TMC-containing hexane (0.2 wt%) was gently poured on top. After 1 min reaction, the syringe-walls were perforated with needles and the reagents were replaced 3 times with fresh clean solvent to remove all reactants. The organic solution and most of the aqueous solution were then removed and finally the seal of the nozzle was broken after which the remaining aqueous solution flowed out and the film settled on the bottom of the syringe. The film was then scraped off and powderized using a mortar. The full experimental setup can be seen in Figure S3.

2.7 Membrane characterization

Filtration

Membrane separation performance was investigated through pressure-driven dead-end filtrations using a high-throughput setup that allows simultaneous testing of up to 16 membranes with one feed. Rose bengal (1017 Da, 35 µM concentration), methyl orange (327 Da, 35 µM) and NaCl (1000 ppm) solutions in MilliQ deionized water (R > 18.2 MΩ.cm) were used as feed. 4 coupons were cut from every membrane to check the reproducibility of the results and to determine standard deviations. Feed pressure was kept constant at 10 bar and the feed solution was stirred at 400 rpm to minimize concentration polarization. Permeate was first discarded to allow the membranes to reach steady state. Thereafter, 3 vials of permeate were collected from every membrane coupon to check if steady state was reached. Weight of the permeate was used to calculate the membrane permeance (P) (using equation (1) with V: permeate volume; A: active membrane area; t: filtration time and ΔP: pressure) and UV-Vis absorbance and conductivity measurements were used to determine the dye and salt retentions (R) respectively, using equation (2) (with C_p and C_f solute concentration in permeate and feed respectively).

$$P = \frac{V}{A \,.t \,.\Delta P} \qquad \text{(equation 1)}$$

$$R = \left(1 - \frac{C_p}{C_f}\right) x\ 100\% \qquad \text{(equation 2)}$$

Scanning Electron Microscopy

Membrane surface and cross-section images were acquired using a JEOL JSM-6010LV SEM operated at an acceleration voltage of 10 kV. Cross-sections were prepared by fracturing the membranes in liquid nitrogen.

Transmission Electron Microscopy

For TEM characterization, membranes were embedded within the epoxy resin EpoFix, followed by ultramicrotomy using an EM FC7 ultramicrotome (Leica Microsystems GmbH, Germany). Sections of a thickness of approximately 40 nm were cut. High Angle Annular Dark Field (HAADF) imaging and Energy Dispersive X-ray spectroscopy (EDX) measurements were performed at 200 kV using a Titan 60-300 microscope (FEI, Thermo Fisher Scientific, USA) equipped with an SuperX EDX detector (Bruker, USA). EDX spectra and MAPS were generated with the Bruker software Esprit. Each membrane cross-section was analyzed at >6 locations to check if the observed findings were valid for the entire area.

X-Ray Diffraction

X-ray diffraction patterns were collected in transmission mode using a STOE Stadi P high-throughput powder diffraction apparatus equipped with a CuKα X-ray tube (λ = 1.5418 Å) and an image plate detector. Obtained diffraction patterns were offset to the theoretically predicted patterns generated based on .CIF files.

X-ray photoelectron spectroscopy

A commercial Omicron XPS system consisting of a non-monochromated DAR 400 X-ray source, an EA 125 electron analyzer and an anode of Mg Kα with radiation at 1253.6 eV were used in this work. UNIFIT was used to fit the XPS spectra. The background, which is subtracted from the spectral peaks, was chosen to be a Shirley type, which removes an iterative background. Overview spectra were collected from 1 sweep, with a step width of 0.2 eV, dwell time of 0.3 s and in constant analyser energy-mode at 50 eV. Detailed spectra were obtained by taking 50 sweeps, with a step width of 0.1 eV and a dwell time of 0.5 s.

Positron Annihilation Lifetime Spectroscopy

Positron annihilation lifetime spectroscopy (PALS) is a well-established tool to measure the free volume in polymer membranes. After thermalization, a positron and an electron can form a hydrogen-like element, the so-called positronium (Ps). It occurs either as para-positronium (p-Ps) in a spin-singlet state or as ortho-positronium (o-Ps) in a spin triplet state. The latter is trapped inside free volume holes until its annihilation with an electron of its surroundings into two gamma-quanta. The average lifetime of the o-Ps, the pick-off lifetime of the o Ps, which can be extracted from the measured spectra, can be directly correlated to the free volume hole size according to the Tao-Eldrup model.[28,29] This model, assuming spherical holes with infinite walls, gives a quantum mechanical description of the correlation of free volume radius and o-Ps lifetime:

$$\tau_3 = {}^1\!/_2 \left[1 - \frac{R}{R+\Delta R} + \frac{1}{2\pi}\sin\left(\frac{2\pi R}{R+\Delta R}\right)\right] \qquad \text{(equation 3)}$$

In this equation τ_3 is the o-Ps lifetime, R the radius of the free volume hole and ΔR the thickness of the electron layer surrounding the free volume hole, which is assumed to be 0.166 nm. This model is valid for lifetimes up to 10 ns, but can be extended to the full lifetime regime.[30] The intensity of the o-Ps is a product of Ps formation probability and the concentration of free volume holes. Therefore, it can be used in some cases to estimate relative changes in the hole concentration.

To measure thin polymer films, an adjustable monoenergetic positron beam is needed, leading to defined implantation profiles,[31] even in multi-layered structures.[32] The pulsed low energy positron beam system (PLEPS), which is operated at the neutron induced positron source Munich (NEPOMUC),[33,34] allows such measurements.[35,36]

The monoenergetic positrons are accelerated to the sample and lose their kinetic energy due to collisions and ionization processes in the first picoseconds after reaching the surface. The length scales of these curves depend on the density of the material and the kinetic energy of the positrons. The resulting implantation profiles in polymers can be calculated according to a well-established procedure.[31] For low energies, the mean implantation depth can be calculated with:

$$z_{mean} = 29.9\frac{E^{1.71}}{\rho} \qquad \text{(equation 4)}$$

where E depicts the implantation energy (keV) and ρ the density (g/cm³).

In this work, all samples were measured at implantation energies of 0.5, 1 and 1.5 keV. The high concentration and reference samples were additionally measured at 0.75 and 1.25 keV to increase depth resolution and to allow intra-sample analysis. For all spectra, 4 million counts were collected with a count rate of about 5000 cts/s and a time resolution of about 250 ps. All spectra were evaluated with LT9.210 and POSWIN. The resolution

function was determined by measuring p-doped SiC, a sample with known lifetimes. The spectra were deconvoluted into four lifetime components (p-Ps, free e+ and two o-Ps) leading to overall fit variances from 1.0 to 1.1.

3. RESULTS AND DISCUSSION

3.1 Theoretical assessment of TFN membrane performance

Although the potential of MOFs in TFN membranes has been widely demonstrated, the exact role of the fillers remains unclear. Ideally, and this is how filler effects are most commonly explained, the filler is incorporated as a porous, low-resistant material allowing increased permeance of at least one compound of the feed mixture. Rejection can originate from both the filler and unchanged toplayer or from the toplayer alone, depending on the solute size and pore aperture size of the filler. When transport in TFN membranes is only governed by these principles, it can be modelled like Mixed Matrix Membranes (MMMs) commonly used in gas separation using e.g. the Maxwell model (see equation 5, with P_c, P_f, and $\emptyset_f$ respectively the continuous and filler phase permeability and the filler volume fraction).[37–39] Although the Maxwell model assumes the filler is ideally embedded within the matrix and as such neglects any matrix-filler interactions, it is known to provide a reasonable fit with experimental data at lower filler loadings.[39,40]

$$P_{composite} = P_c \left[\frac{P_f + 2P_c - 2\emptyset_f (P_c - P_f)}{P_f + 2P_c + \emptyset_f (P_c - P_f)} \right] \qquad \text{(equation 5)}$$

With a hypothetical PA permeability of 1 arbitrary unit (a.u.) and a filler permeability of 10 a.u., the modelled permeability of the composite toplayer is plotted in Figure 1. It can be seen that in order to have a permeance increase in the order of e.g. +160%, as observed by Duan et al. (2015),[12] a filler fraction of >40% would be required. However, neither XPS nor TEM analysis indicate the presence of such large amounts of filler in their membranes. Similar observations can be made for most, if not all, TFN membranes. Our

previous work on EFP-based TFN membranes also did not show a degree of filler incorporation that could explain the observed permeance increase.[10]

TFN membranes can also be prepared using dense filler particles, e.g. aimed at reducing fouling or incorporating antimicrobial properties in the membrane.[41] Permeance of such TFN-membranes should actually decrease if only the above discussed ideal effects are taken into account. However, often also these membranes show permeance and/or rejection changes upon filler addition. E.g., Kim et al. (2012) observed an increase in permeance when incorporating (non-porous) silver nanoparticles to prepare a TFN membrane.[42]

These findings suggest that apart from the ideal or primary filler effects, secondary effects could play a very, if not the most, important role. Such effects could be of various origin. It has been suggested that hydratation of filler particles once they come into contact with the aqueous phase during the IP, could result in the local generation of heat which will influence the IP-kinetics and solvent miscibility.[43] Many of the filler materials used in TFN synthesis are known to have catalytically active surfaces, possibly influencing the IP as well. Another possible effect could be degradation of the filler. Indeed, the most commonly used condensation polymerization reaction between an acid chloride and a diamine results in the formation of HCl (Figure 1). Since an IP reaction is highly localized and fast, the local pH is expected to drop quite dramatically which could result in the degradation of acid sensitive materials as observed experimentally for $Cd(OH)_2$ by Karan et al. (2016).[6] ZIF-8, although considered to be one of the more stable MOFs, already starts to degrade at pH 5.[44–47] As such, it could very well be that apart from filler particles, also particle fragments and degradation products (in the case of MOFs: free metal ions

and linkers) are present at the interface during IP. Although the generation of HCl is inherently connected to the use of the diamine / acyl chloride IP chemistry, its effect could possibly be remediated through the use of acid quenching additives (e.g. TEA) or completely omitted through the use of other IP chemistries that do not generate HCl as a side product. Jimenez-Solomon et al. for instance report the formation of high free-volume polyarylate toplayers through the use of alcohol functional monomers.[7] As NaOH is added to the aqueous phase to deprotonate the alcohol functions to increase their reactivity, the IP reaction with TMC only forms NaCl as side product instead of HCl. As such this could provide an alternative for the acid-generating diamine / acyl chloride chemistry for specific cases (such as e.g. ZIF-8) where the filler is known to be stable in alkaline conditions.[48]

To investigate this disparity between theoretically predicted (based solely on primary filler effects) and observed membrane performance (influenced by both primary and secondary effects), the power of nanoscale visualization and chemical characterization via STEM, crystallographic analysis via XRD, free volume analysis via PLEPS and directed synthesis experiments was combined.

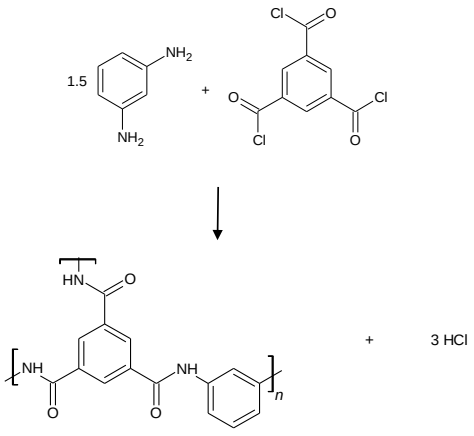

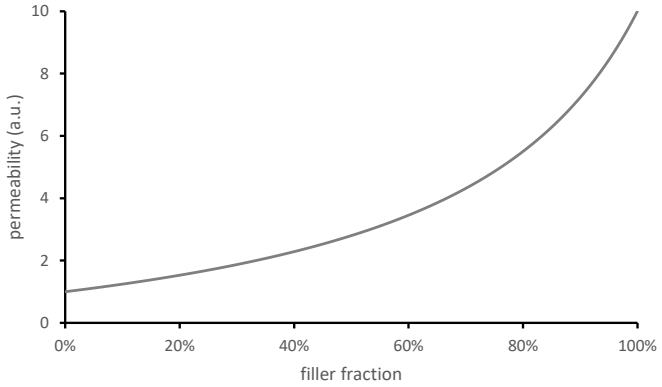

Figure 1. (left) The (interfacial) condensation polymerization reaction between TMC and MPD which forms a cross-linked PA network and HCl. (right) Maxwell prediction for the permeability of a composite phase with $P_{continuous} = 1$ and $P_{dispersed} = 10$.

3.2 STEM characterization

Our previously reported EFP-based TFN membranes showed extremely high permeance increases with almost no filler present in the synthesis solutions (i.e. 0.005 w/v% ZIF-8). However, hardly any Zn was found back in the membranes through XPS analysis (< 0.15 atom%). The TEM images revealed dark and sharp-edged features which were assumed to be the ZIF-8 particles, but this could not be proven without the use of spatially resolved analytical tools.[10] State-of-the-art HAADF-STEM allows Z-contrast imaging of materials at the nanoscale in combination with spatially resolved spectroscopic tools (STEM-EDX/EELS).[26,49] The EFP-based membrane which showed the highest permeance increase (0.005 w/v%) and a membrane prepared with a much higher ZIF-8 concentration (0.1 w/v%) were analyzed and compared using HAADF-STEM imaging in combination with Zn mapping via EDX. EDX mapping of nitrogen and sulfur on the 0.005 w/v% ZIF-EFP membrane was used to confirm the boundaries of the PA toplayer on the HAADF-STEM image (see Figure S4). The HAADF-STEM image (Figure 2a) shows a 300 nm thick toplayer that formed on top of the support. The ridge-and-valley structure that is typical for regular PA TFC membranes can be seen.[4] Multiple areas of this membrane cross-section were analyzed via EDX for the presence of Zn. However, no Zn above the detection limit (typically < 0.03 wt% for a Chemistem detector) was found (a typical EDX spectrum is shown in Figure 2b). This is in accordance with the XPS analysis

of the top surface of this sample which showed an almost negligible Zn concentration of 0.15 atom%.

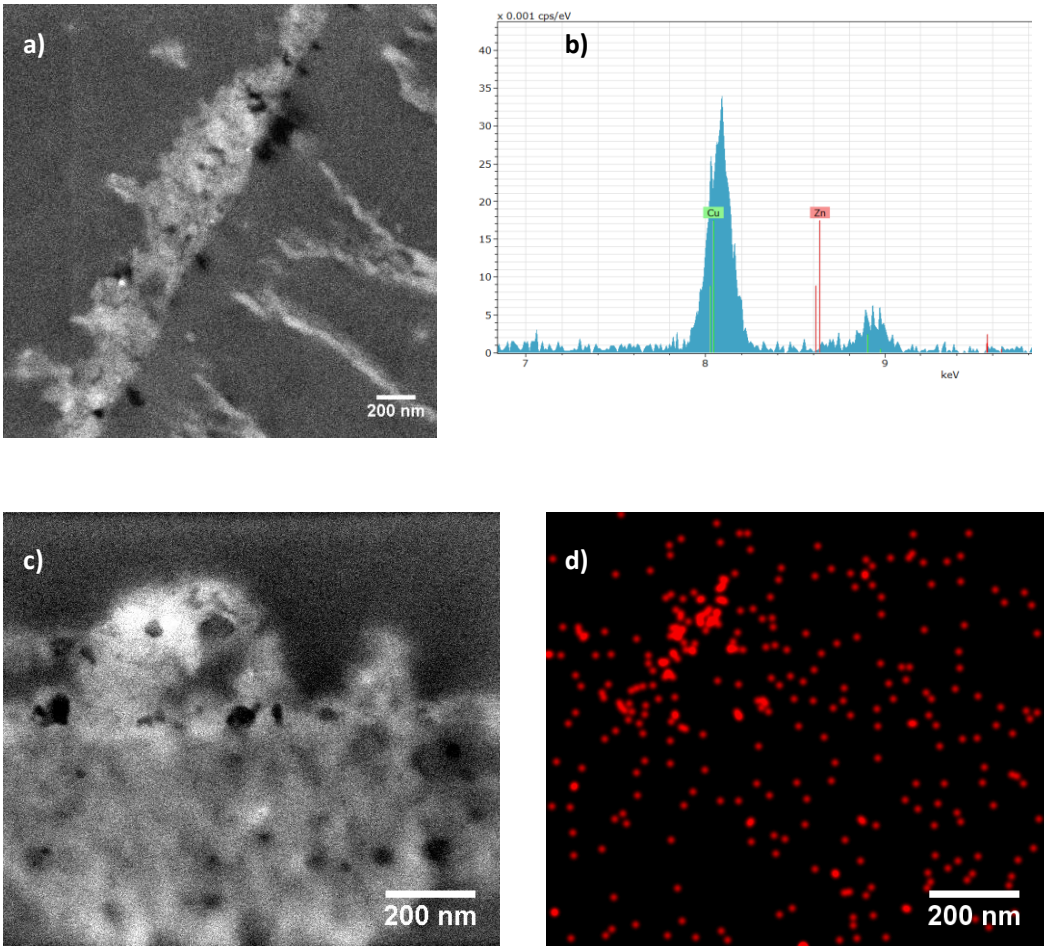

Figure 2. HAADF-STEM cross-section image of the 0.005 w/v% ZIF-EFP membrane (a) and part of the EDX spectrum taken from this area (b) (Cu signal originates from the TEM-grid). (c) HAADF-STEM image of the 0.1 w/v% ZIF-EFP membrane and (d) the STEM-EDX mapping of this area.

The highly loaded ZIF-EFP membrane prepared with 0.1 w/v% ZIF-8 in the synthesis solution was analyzed similarly to investigate whether a higher ZIF-8 concentration in the synthesis would result in an enhanced incorporation and hence in a detectable Zn signal.

Although the XPS analysis did not show a higher Zn concentration, the STEM-EDX-mapping did reveal areas with detectable Zn-concentrations. As can be seen from Figure 2d, few small (< 50 nm) areas with elevated Zn-concentrations were detected close to each other (the randomly distributed signal is noise on the measurement). Such groups of small areas with elevated Zn concentrations were found at several spots along the membrane toplayer (see Figure S5). However, these areas were consistently smaller than the 150 nm diameter of the ZIF-8 particles and featured a more elongated shape following the contours of the PA toplayer. This could suggest that these are not whole ZIF-8 particles but rather particle fragments that are spread throughout the toplayer, which accords with the hypothesis postulated above that the acid generated during the IP could degrade the ZIF-8 nanoparticles.

3.3 Influence of the presence of Zn^{2+} on the IP process

The presence of what appears to be degradation fragments of the filler particles on the Zn-mappings of the EFP-TFN membranes, suggests that, apart from filler particles, also degraded fragments thereof and maybe even free Zn^{2+} and Mim^- could locally be present near the interface in significant amounts during the IP. These compounds could thus also influence the IP reaction, but in a completely different way than how could be expected from a MOF particle. Indeed, Lewis acids such as Zn^{2+}, are known to activate carbonyl compounds, such as acid halides (e.g. in Friedel Crafts acylation reactions) and their presence at the interface could thus promote the reactivity of the acid chloride monomer.[50,51] Although Zn^{2+} is not the strongest Lewis acid (cations such as Al^{3+} or Ca^{2+} are stronger), the influence of Zn^{2+} was further investigated to create similar conditions to the synthesis of ZIF-8 TFN membranes. As the catalytic effect of the Lewis acid promote

both the reaction of the TMC with MPD (the aimed condensation polymerization) or with H_2O (the TMC hydrolysis side reaction), it can have different effects on the membrane performance. If the TMC hydrolysis would be promoted, the Zn^{2+} would have a catalytic effect on the ZIF-8 degradation as a higher rate of TMC hydrolysis would result in an even higher rate of HCl acid generation. This would result in a very unselective toplayer as the reaction between trimesic acid and MPD is not favorable. The IP reaction is supposed to take place in the organic phase, but it is postulated that most of the Zn^{2+} released by filler breakdown readily moves to the aqueous phase because of the low solubility of ionic species in the apolar organic phase. Thus, to probe for the possible influence of Zn^{2+} on the IP reaction, $Zn(NO_3)_2.6H_2O$ was added to the aqueous amine phase during TFC membrane synthesis. The prepared membranes, further denoted as Zn-TFCs, were characterized through aqueous filtrations using methyl orange and NaCl as solutes (Figure 3a).

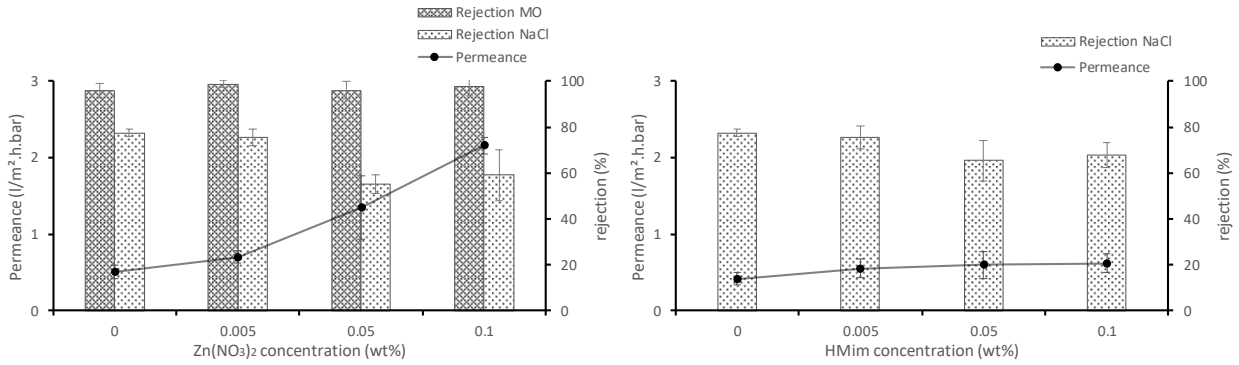

Figure 3. Permeance and NaCl/MO rejection for (a) Zn-TFC and (b) HMim-TFC membranes prepared with various concentrations Zn / HMim in the aqueous phase during synthesis. The lines were added to guide the viewer. Experiments were performed at 10 bar, 25°C using 1 g/l NaCl or 35 µM MO in H_2O.

The water permeance increases proportionally with the Zn^{2+} concentration in the aqueous phase. The NaCl retention of the reference TFC membrane is 78%, which is not as high as high as typical lab-made and industrial TFC RO membranes. However, such retention is useful in present work, as it allows to easily observe both increases and decreases in salt rejections. The rejection of the Zn-TFC membranes drops from 78% to 59% with increasing Zn^{2+} concentration, while the MO retention does not change drastically. This could suggest that the presence of the Zn^{2+} ions slightly decreases the tightness of the PA network in the toplayer. Fan et al. (2014) observed similar results when investigating the effect of adding $CaCl_2$ to the aqueous phase in IP.[52] The similarly small loss in retention combined with a permeance increase was attributed to Ca^{2+} (also a Lewis acid) promoting the TMC hydrolysis, resulting in the formation of a more loose PA layer. However, no XPS was performed to support this hypothesis and the interaction volume of the reported EDX is too big to draw conclusions on the chemical composition of the toplayer and can thus not provide evidence to support the hydrolysis hypothesis. The prepared Zn-TFCs were analyzed using XPS to assess the influence of the Zn^{2+} on the chemistry of the formed toplayer (see Table 1). The Zn-TFC membrane shows a lower O/N ratio, reflecting a higher crosslinking degree of the toplayer,[53] which indicates that the Zn^{2+} activates the TMC preferentially towards IP and thus does not promote hydrolysis of the acyl chloride groups. The higher permeance of the Zn-TFC membranes can then most probably be explained by the formation of a thinner toplayer, assuming similar chemical interactions. Unfortunately, it was not possible to statistically prove this via TEM because of the high intra-sample variation intrinsic to most PA films prepared via IP. The small decrease in salt retention possibly originates from the thinner toplayer, being more

prone towards defects. The morphology of these Zn-TFC membranes was further characterized through SEM and STEM. Top-view SEM images show (Figure 4a) that the TFC membrane prepared in the absence of Zn has the typical rough ridge-and-valley structure, just as the 0.005 w% Zn-based membrane. However, a further increase of the Zn concentration leads to a drastic decrease in size and appearance of these surface features, resulting in a more crater-like surface. A representative HAADF-STEM image and STEM-EDX based Zn mapping of the 0.1 w% Zn-TFC membrane are shown in Figure 4b. No Zn could be detected in the PA toplayer (also in XPS, no Zn could be detected). These results show that very low Zn concentrations, well below the detection limits of modern analytical techniques applicable to membranes, can already induce very large differences in membrane structure and performance.

Table 1. O/N ratio determined via elemental analysis using XPS for the Zn-TFC and the reference TFC membrane.

Sample	**O/N**
Reference TFC	1.20
Zn-TFC	1.06

The increased degree of crosslinking that was observed for the Zn-TFC membranes was however not observed for the EFP-TFN membranes (XPS data, see supporting information). A possible explanation for this can be found in the hindered diffusion of the monomers by the presence of the nanoparticles during the IP of the EFP-TFN membranes.

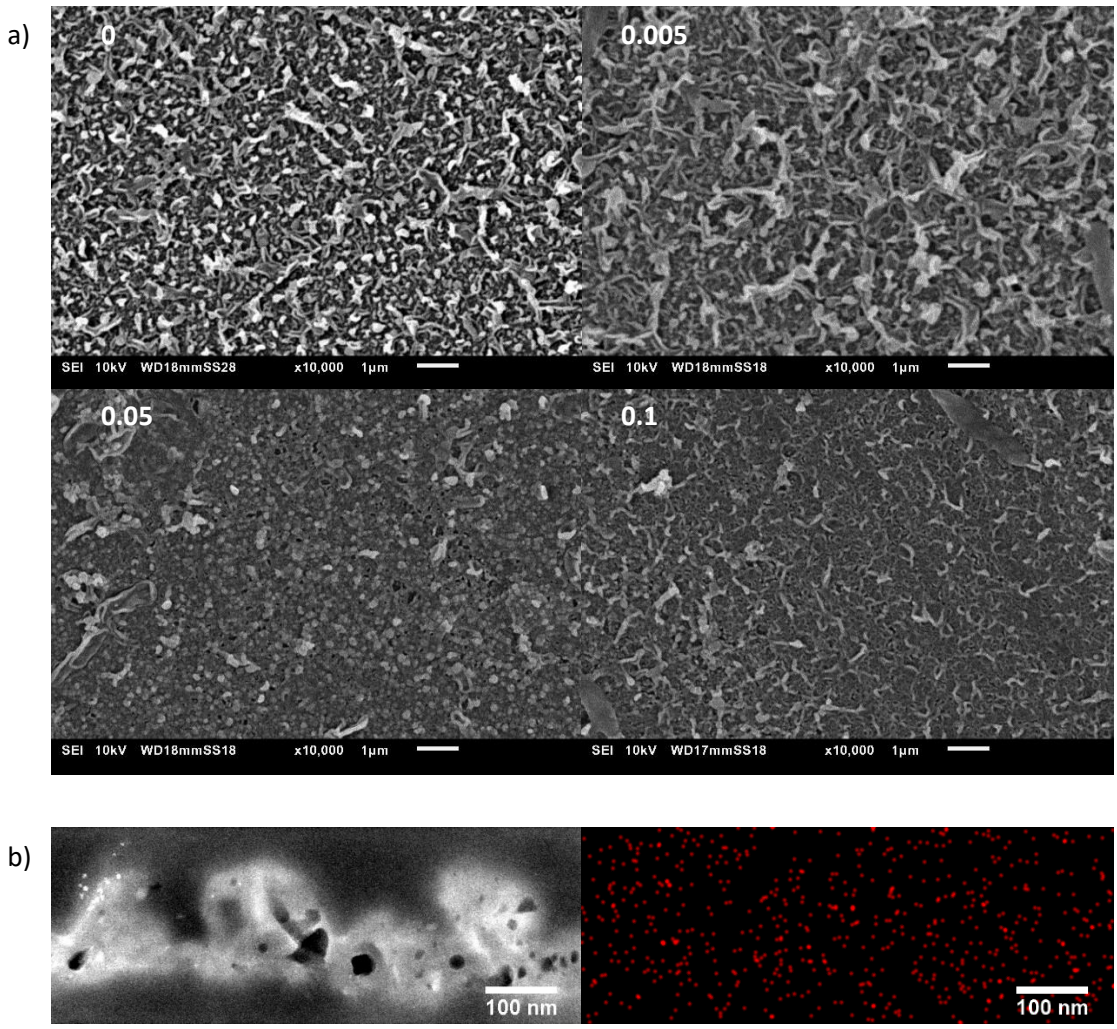

Figure 4. (a) SEM topview images of the Zn-TFC membranes (Zn concentration in w/v% indicated on the respective images) and (b) HAADF-STEM cross-section image and STEM-EDX Zn mapping of the 0.1 w/v% Zn-TFC membrane.

The possible influence of the other potential break-down product HMim on the formation of TFC membranes was also investigated. Mim^- liberated during breakdown of ZIF-8 can act as a weak base, HMim-TFC membranes were thus prepared, similar to the Zn-TFC membranes. Although the addition of HMim might not have the same effect as Mim^-, HMim seemed the best choice because of the unknown effect of the inevitable cation associated to Mim^-. The filtration results of these membranes are shown in Figure 3b. Increasing the HMim concentration in the aqueous solution from 0 to 0.1 w% does not result in a statistically different permeance, while salt rejection decreases from 78 to 68%. SEM topview images of the membranes showed the standard ridge-and-valley morphology and little variation between the different samples (see Figure S6). The magnitude of the changes when dosing HMim in TFC membrane synthesis is clearly much smaller than for Zn^{2+}.

3.4 XRD analysis

As ZIF-8 is a crystalline material, further evidence to support the hypothesis that the fillers degrade from the acid generated during the IP can be sought through XRD. Free-standing PA-films with and without ZIF-8 were prepared and grinded, after which the resulting powder was analysed via XRD to check for the presence of crystalline particles in the polymer matrix. The resulting diffraction patterns are shown in Figure 5a. Unfilled PA shows a diffraction pattern typical for an amorphous polymer with no well-defined peaks. The diffraction pattern of the filled PA shows some ill-defined, low-intensity peaks. Comparison with the theoretical diffraction pattern of ZIF-8 doesn't show a clear match between the observed and predicted peaks. As such, this result could either support the

hypothesis that ZIF-8 is at least partly broken down during the IP reaction or it could be a consequence of the too low amount of ZIF-8 that is effectively incorporated in the thin PA film. To discriminate between both hypotheses, a control experiment was executed. The synthesis of TFC membranes for application in RO in the conventional hexane-water system requires the use of additives.[5] One of the additives often used is the base triethylamine (TEA) which acts both as a quencher for the protons generated in the IP and as catalyst for the condensation polymerization reaction between TMC and MPD.[5] Since TEA quenches the generated protons, it is presumed that, in the presence of TEA, the pH at the interface will locally become less acidic than without the additive. It is therefore expected that the addition of the base will result in reduced filler degradation. A free-standing film with TEA in the aqueous amine solution and ZIF-8 in the organic phase was thus synthesized and analysed via XRD. The diffraction pattern with TEA shows a relatively strong reflection at 7.3° that can be attributed to ZIF-8 and several lower intensity reflections. However, still no long range order could be detected. Since the same concentration of ZIF-8 was used in the preparation of this sample and since the same amount of sample was used for XRD analysis, this suggests that the incorporated ZIF-8 indeed retains more of its crystallinity throughout the IP when using TEA and hence that it is highly probably that ZIF-8 is (at least partially) broken down during the IP.

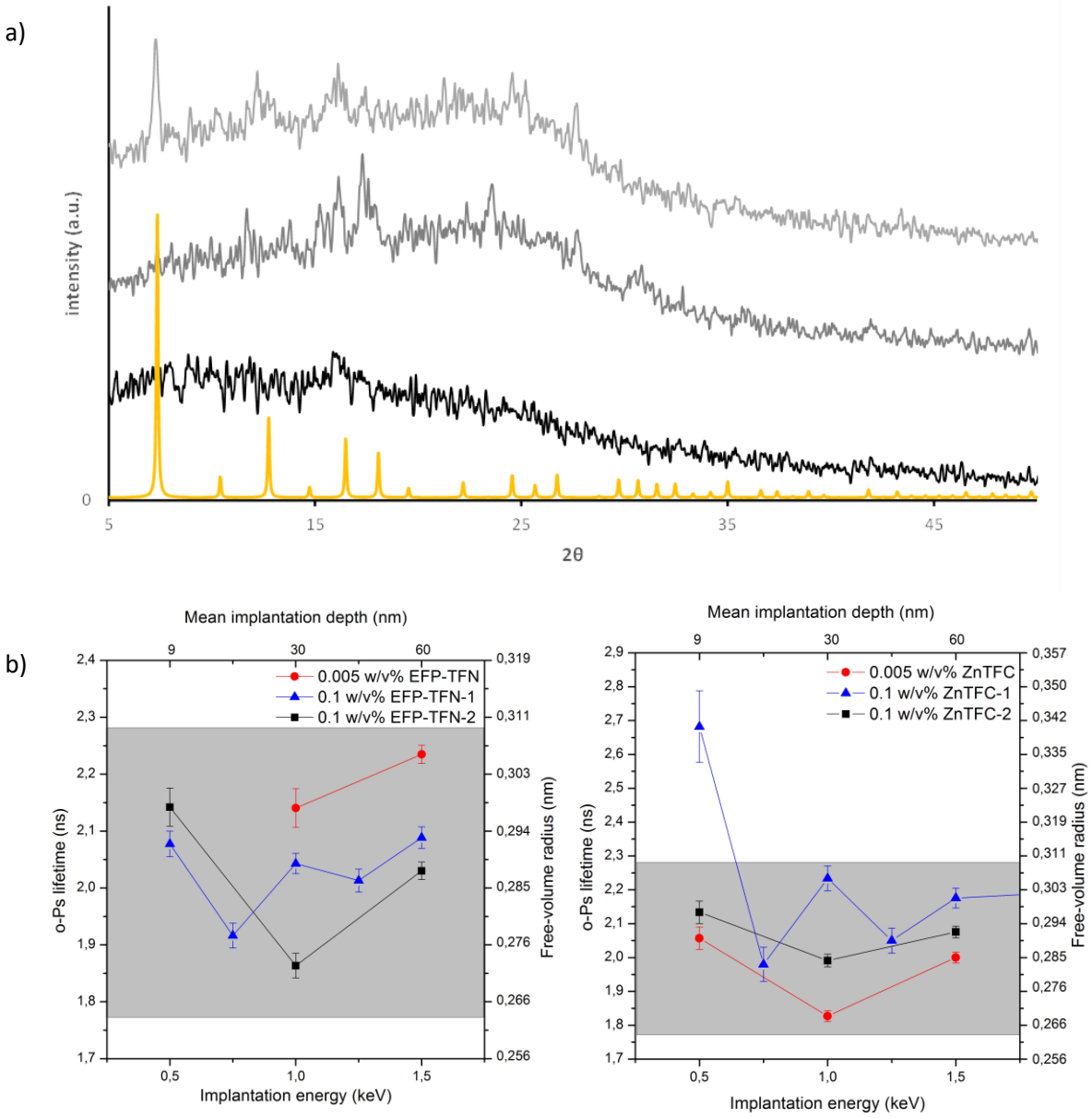

Figure 5. (a) X-ray diffraction patterns of regular PA (black), PA prepared with ZIF-8 (grey), PA prepared with ZIF-8 and TEA (light grey) and a theoretical powder diffraction pattern of ZIF-8 (yellow). Spectra are shifted vertically for clarity. (b) o-Ps lifetime spectra of EFP-TFN and Zn-TFC membranes. The grey boxes represent the variability measured in the reference TFC membrane.

3.5 PALS analysis

PALS yields sub-nm information regarding the internal free-volume structure of the top layer, a parameter which is believed to strongly influence transport properties of the membrane. This technique thus complements the information obtained via the filtration experiments, the nm-scale structural and chemical characterization via electron microscopy and the analysis of crystalline regions via XRD.

In order to investigate whether the presence of ZIF-8 or its degradation fragments influences the free-volume structure of the PA top layer, first a reference TFC sample was analysed. This was done at three different spots to account for intra-sample variations. The o-Ps lifetime and intensity are shown in Figure S7. o-Ps lifetime can be directly related to free-volume element size, while no direct correlation between o-Ps intensity and porosity exists due its dependence on the probability of o-Ps formation.[54] The average free-volume element sizes range from about 5 to 6 Å, in accordance with literature.[55] However, a large spread on the data is present, which is probably due to the intrinsic ridge-and-valley structure of a typical PA membrane. The rough surface influences the implantation profile of the positrons and also exacerbates surface effects. The data obtained at an implantation energy of 0.5 keV, corresponding to a mean implantation depth of about 9 nm, should hence not be taken into further consideration. At an implantation energy of 1.5 keV, the influence of the support becomes visible, as intensity values sharply increase. Therefore, in order to be able to fully associate the obtained o-Ps lifetime to the internal structure of the PA top layer, it is best to focus on the values obtained between 0.75 and 1.25 keV.

In Figure 5b, the o-Ps lifetime data from the EFP and Zn-TFC membranes are shown and compared to the reference TFC membrane, of which the data is presented via the

grey rectangle (the intensity profiles can be found in Figure S8). The size of free-volume elements of both the Zn-TFC and EFP membranes is not significantly different from the reference TFC membranes, as all data points overlap. The same holds true for o-Ps intensity. This means that there is no quantitative proof that the presence of either pure Zn-ions (Zn-TFC membranes) or ZIF-8 nanoparticles or degradation fragments thereof (EFP-membranes) during the synthesis process significantly alters the free-volume structure of the PA top layer. Additionally, for the EFP-membranes, the typical cavities of ZIF-8 with a diameter of about 11.6 Å[56] could neither be detected in the lifetime spectrum, even though these can be probed with PALS.[57] This indicates that either the ZIF-8 particles were degraded during IP or that the incorporated amount is too low to produce a significant o-Ps annihilation signal.

The changes in membrane performance after the addition of Zn ions or ZIF-8 NPs during the synthesis procedure can thus not be related to the PA's free-volume structure. This is rather surprising as free-volume element size is an important parameter governing transport through the active membrane layer, as included in the thermodynamic diffusion coefficient of the solution-diffusion model.[58] It is therefore believed that PALS on samples with high intra-sample variations regarding top-layer roughness and thickness is not ideal and can (partially) be held responsible for the non-existing correlation between free-volume and membrane performance. These structural differences are, as discussed before, very obvious from SEM top-view images but thus remain very difficult to characterise quantitatively with the currently available techniques. A tool allowing membrane cross-sections with TEM resolution on a very large sample volume would be

extremely valuable for the membrane community to obtain a better insight in the top-layer structure and hence, amongst others, in the role of fillers in TFN membranes.

4. CONCLUSION

The formation of interfacially polymerised TFN membranes prepared via the EFP method was investigated at nanoscale combining several approaches to investigate the influence of so-called secondary effects on the IP. A detailed morphological and compositional characterization was done through HAADF-STEM. The analysis revealed a toplayer morphology very similar to regular TFC membranes but no direct observations of incorporated filler particles could be made. EDX-mapping of Zn in the nanocomposite toplayers revealed the presence of small zones with elevated Zn concentrations, ascribed to ZIF-8 fragments and molecular degradation products thereof which are formed under the locally very acidic conditions created during the IP.

The effect of the two possible breakdown products of ZIF-8, Zn^{2+} and 2-methylimidazole, on the IP was investigated separately and showed that mainly Zn^{2+} has a permeance increasing effect with a small loss of rejection at higher concentrations. The surface morphology of the Zn-TFC membranes was found to be similar to EFP-based TFN membranes. 2-methylimidazole had no significant effect on permeance and rejection.

The possible filler degradation during IP was further investigated through the analysis of diffraction patterns obtained from free standing films, which clearly showed a more clear diffraction signal when the free-standing film was prepared in the presence of the acid quenching TEA. This confirmed the potential degrading effect of the acid generated during the IP on the acid sensitive filler.

Using PALS, it was not possible to show a significant difference between the reference TFC membrane and the EFP-TFN or Zn-TFC membrane. This was attributed to rough

and variable surface structure of the membrane toplayers which is not ideal for PALS analysis.

Although PALS experiments were not fully conclusive due to intrinsic sample and technique limitations, insights from all experiments strongly imply that ZIF-8 is partly degraded during IP and that the secondary effects resulting from the presence of degradation products contribute to the drastic performance changes that are typically observed. Systematic characterization of systems using other types of fillers and IP chemistries would certainly further benefit the design and understanding of the exact functioning of TFN membranes.

The herein presented results show for the first time that the role of MOFs, and possible also other filler types, in TFN membranes is more complex than commonly accepted. Not only the porosity, but also the other properties of the material such as its stability window or catalytic effects influence the formation and functioning of TFN membranes. By extension, these findings are also crucial for all research on composites based on MOFs (and other materials). Whereas the effects of many synthesis methods for composite materials will be limited to less detrimental effects such as e.g. Ostwald ripening,[59] also the application of the materials should be critically addressed as often envisaged applications might not fall within the long term stability window of the material.

ACKNOWLEDGMENTS

C.V.G. and R.V. kindly acknowledge respectively the Flemish Agency for Innovation through Science and Technology (IWT) and the Flemish Fund for Scientific Research (FWO, 1S00917N) for a PhD scholarship. The authors kindly acknowledge funding from KU Leuven through C16/17/005 and from the Belgian Federal Government through IAP 6/27 Functional Supramolecular systems. S.B. and M.P. acknowledge financial support from the European Research Council (ERC Starting Grant #335078-COLOURATOM). M.P. acknowledges funding from the European Union (ESTEEM2, No. 312483) and the HEiKA centre FunTECH-3D. The MLZ-Garching is kindly acknowledged for providing access to the NEPOMUC facilities (project n°11541).

ABBREVIATIONS

EDX, Energy Dispersive X-ray spectroscopy; HAADF, High-Angle Annular Dark Field; HMim, 2-methylimidazole; IP, Interfacial Polymerization; PALS, Positron Annihilation Lifetime Spectroscopy; SEM, Scanning Electron Microscopy; (S)TEM, (Scanning) Transmission Electron Microscopy; TFC, Thin-Film Composite; TFN, Thin-Film Nanocomposite; XRD, X-Ray Diffraction.

REFERENCES

(1) Hermans, S.; Mariën, H.; Van Goethem, C.; Vankelecom, I. F. Recent Developments in Thin Film (Nano)composite Membranes for Solvent Resistant Nanofiltration. *Curr. Opin. Chem. Eng.* **2015**, *8*, 45–54.

(2) Vandezande, P.; Gevers, L. E. M.; Vankelecom, I. F. J. Solvent Resistant Nanofiltration: Separating on a Molecular Level. *Chem. Soc. Rev.* **2008**, *37* (2), 365–405.

(3) Marchetti, P.; Jimenez Solomon, M. F.; Szekely, G.; Livingston, A. G. Molecular Separation with Organic Solvent Nanofiltration: A Critical Review. *Chem. Rev.* **2014**, *114* (21), 10735–10806.

(4) Hermans, S.; Bernstein, R.; Volodin, A.; Vankelecom, I. F. J. Study of Synthesis Parameters and Active Layer Morphology of Interfacially Polymerized Polyamide–polysulfone Membranes. *React. Funct. Polym.* **2015**, *86*, 199–208.

(5) Mariën, H.; Bellings, L.; Hermans, S.; Vankelecom, I. F. J. Sustainable Process for the Preparation of High-Performance Thin-Film Composite Membranes Using Ionic Liquids as the Reaction Medium. *ChemSusChem* **2016**, *9* (10), 1101–1111.

(6) Karan, S.; Jiang, Z.; Livingston, A. G. Sub-10 Nm Polyamide Nanofilms with Ultrafast Solvent Transport for Molecular Separation. *Science* **2015**, *348* (6241), 1347–1351.

(7) Jimenez-Solomon, M. F.; Song, Q.; Jelfs, K. E.; Munoz-Ibanez, M.; Livingston, A. G. Polymer Nanofilms with Enhanced Microporosity by Interfacial Polymerization. *Nat. Mater.* **2016**, *15* (7), 760–767.

(8) Jeong, B.-H.; Hoek, E. M. V.; Yan, Y.; Subramani, A.; Huang, X.; Hurwitz, G.;

Ghosh, A. K.; Jawor, A. Interfacial Polymerization of Thin Film Nanocomposites: A New Concept for Reverse Osmosis Membranes. *J. Memb. Sci.* **2007**, *294* (1–2), 1–7.

(9) Lau, W. J.; Gray, S.; Matsuura, T.; Emadzadeh, D.; Paul Chen, J.; Ismail, A. F. A Review on Polyamide Thin Film Nanocomposite (TFN) Membranes: History, Applications, Challenges and Approaches. *Water Res.* **2015**, *80*, 306–324.

(10) Van Goethem, C.; Verbeke, R.; Hermans, S.; Bernstein, R.; Vankelecom, I. F. J. Controlled Positioning of MOFs in Interfacially Polymerized Thin-Film Nanocomposites. *J. Mater. Chem. A* **2016**, *4* (42), 16368–16376.

(11) Sorribas, S.; Gorgojo, P.; Téllez, C.; Coronas, J.; Livingston, A. G. High Flux Thin Film Nanocomposite Membranes Based on Metal-Organic Frameworks for Organic Solvent Nanofiltration. *J. Am. Chem. Soc.* **2013**, *135* (40), 15201–15208.

(12) Duan, J.; Pan, Y.; Pacheco, F.; Litwiller, E.; Lai, Z.; Pinnau, I. High-Performance Polyamide Thin-Film-Nanocomposite Reverse Osmosis Membranes Containing Hydrophobic Zeolitic Imidazolate Framework-8. *J. Memb. Sci.* **2015**, *476*, 303–310.

(13) Wang, L.; Fang, M.; Liu, J.; He, J.; Li, J.; Lei, J. Layer-by-Layer Fabrication of High-Performance Polyamide/ZIF-8 Nanocomposite Membrane for Nanofiltration Applications. *ACS Appl. Mater. Interfaces* **2015**, *7* (43), 24082–24093.

(14) Wang, L.; Fang, M.; Liu, J.; He, J.; Deng, L.; Li, J.; Lei, J. The Influence of Dispersed Phases on polyamide/ZIF-8 Nanofiltration Membranes for Dye Removal from Water. *RSC Adv.* **2015**, *5* (63), 50942–50954.

(15) Reinsch, H.; Bueken, B.; Vermoortele, F.; Stassen, I.; Lieb, A.; Lillerud, K.-P.; De Vos, D. Green Synthesis of Zirconium-MOFs. *CrystEngComm* **2015**, *17* (22), 4070–

4074.

(16) Echaide-Górriz, C.; Sorribas, S.; Téllez, C.; Coronas, J. MOF Nanoparticles of MIL-68(Al), MIL-101(Cr) and ZIF-11 for Thin Film Nanocomposite Organic Solvent Nanofiltration Membranes. *RSC Adv.* **2016**, *6* (93), 90417–90426.

(17) Ma, D.; Peh, S. B.; Han, G.; Chen, S. B. Thin-Film Nanocomposite (TFN) Membranes Incorporated with Super-Hydrophilic Metal-Organic Framework (MOF) UiO-66: Toward Enhancement of Water Flux and Salt Rejection. *ACS Appl. Mater. Interfaces* **2017**, *9* (8), 7523–7534.

(18) Zhu, J.; Qin, L.; Uliana, A.; Hou, J.; Wang, J.; Zhang, Y.; Li, X.; Yuan, S.; Li, J.; Tian, M.; Lin, J.; Van der Bruggen, B. Elevated Performance of Thin Film Nanocomposite Membranes Enabled by Modified Hydrophilic MOFs for Nanofiltration. *ACS Appl. Mater. Interfaces* **2017**, *9* (2), 1975–1986.

(19) Wang, J.; Wang, Y.; Zhang, Y.; Uliana, A.; Zhu, J.; Liu, J.; Van Der Bruggen, B. Zeolitic Imidazolate Framework/Graphene Oxide Hybrid Nanosheets Functionalized Thin Film Nanocomposite Membrane for Enhanced Antimicrobial Performance. *ACS Appl. Mater. Interfaces* **2016**, *8* (38), 25508–25519.

(20) Navarro, M.; Benito, J.; Paseta, L.; Gascón, I.; Coronas, J.; Téllez, C. Thin-Film Nanocomposite Membrane with the Minimum Amount of MOF by the Langmuir-Schaefer Technique for Nanofiltration. *ACS Appl. Mater. Interfaces* **2018**, *10* (1), 1278–1287.

(21) Sarango, L.; Paseta, L.; Navarro, M.; Zornoza, B.; Coronas, J. Controlled Deposition of MOFs by Dip-Coating in Thin Film Nanocomposite Membranes for Organic Solvent Nanofiltration. *Journal of Industrial and Engineering Chemistry*.

2017.

(22) Mitchell, G. E.; Mickols, B.; Hernandez-Cruz, D.; Hitchcock, A. Unexpected New Phase Detected in FT30 Type Reverse Osmosis Membranes Using Scanning Transmission X-Ray Microscopy. *Polymer (Guildf).* **2011**, *52* (18), 3956–3962.

(23) Pacheco, F. A.; Pinnau, I.; Reinhard, M.; Leckie, J. O. Characterization of Isolated Polyamide Thin Films of RO and NF Membranes Using Novel TEM Techniques. *J. Memb. Sci.* **2010**, *358* (1–2), 51–59.

(24) Pacheco, F.; Sougrat, R.; Reinhard, M.; Leckie, J. O.; Pinnau, I. 3D Visualization of the Internal Nanostructure of Polyamide Thin Films in RO Membranes. *J. Memb. Sci.* **2016**, *501*, 33–44.

(25) Kłosowski, M. M.; McGilvery, C. M.; Li, Y.; Abellan, P.; Ramasse, Q.; Cabral, J. T.; Livingston, A. G.; Porter, A. E. Micro-to Nano-Scale Characterisation of Polyamide Structures of the SW30HR RO Membrane Using Advanced Electron Microscopy and Stain Tracers. *J. Memb. Sci.* **2016**, *520*, 465–476.

(26) Van Tendeloo, G.; Bals, S.; Van Aert, S.; Verbeeck, J.; Van Dyck, D. Advanced Electron Microscopy for Advanced Materials. *Adv. Mater.* **2012**, *24* (42), 5655–5675.

(27) Wee, L. H.; Lescouet, T.; Ethiraj, J.; Bonino, F.; Vidruk, R.; Garrier, E.; Packet, D.; Bordiga, S.; Farrusseng, D.; Herskowitz, M.; Martens, J. A. Hierarchical Zeolitic Imidazolate Framework-8 Catalyst for Monoglyceride Synthesis. *ChemCatChem* **2013**, *5* (12), 3562–3566.

(28) Tao, S. J. Positronium Annihilation in Molecular Substances. *J. Chem. Phys.* **1972**, *56* (11), 5499–5510.

(29) Eldrup, M.; Lightbody, D.; Sherwood, J. N. The Temperature Dependence of Positron Lifetimes in Solid Pivalic Acid. *Chem. Phys.* **1981**, *63* (1–2), 51–58.

(30) T. L. Dull; W. E. Frieze, and; Gidley*, D. W.; and, J. N. S.; Yee, A. F. Determination of Pore Size in Mesoporous Thin Films from the Annihilation Lifetime of Positronium. **2001**.

(31) Algers, J.; Sperr, P.; Egger, W.; Kögel, G.; Maurer, F. H. J. Median Implantation Depth and Implantation Profile of 3–18 keV Positrons in Amorphous Polymers. *Phys. Rev. B* **2003**, *67* (12), 125404.

(32) Vehanen, A.; Saarinen, K.; Hautojärvi, P.; Huomo, H. Profiling Multilayer Structures with Monoenergetic Positrons. *Phys. Rev. B* **1987**, *35* (10), 4606–4610.

(33) Hugenschmidt, C.; Dollinger, G.; Egger, W.; Kögel, G.; Löwe, B.; Mayer, J.; Pikart, P.; Piochacz, C.; Repper, R.; Schreckenbach, K.; Sperr, P.; Stadlbauer, M. Surface and Bulk Investigations at the High Intensity Positron Beam Facility NEPOMUC. *Appl. Surf. Sci.* **2008**, *255* (1), 29–32.

(34) Hugenschmidt, C.; Piochacz, C.; Reiner, M.; Schreckenbach, K. The NEPOMUC *Upgrade* and Advanced Positron Beam Experiments. *New J. Phys.* **2012**, *14* (5), 55027.

(35) Egger, W.; Sperr, P.; Kögel, G.; Dollinger, G. Pulsed Low Energy Positron System (PLEPS) at the Munich Research Reactor FRM II. *Phys. status solidi* **2007**, *4* (10), 3969–3972.

(36) Sperr, P.; Egger, W.; Kögel, G.; Dollinger, G.; Hugenschmidt, C.; Repper, R.; Piochacz, C. Status of the Pulsed Low Energy Positron Beam System (PLEPS) at the Munich Research Reactor FRM-II. *Appl. Surf. Sci.* **2008**, *255* (1), 35–38.

(37) de Clippel, F.; Khan, A. L.; Cano-Odena, A.; Dusselier, M.; Vanherck, K.; Peng, L.; Oswald, S.; Giebeler, L.; Corthals, S.; Kenens, B.; Denayer, J. F. M.; Jacobs, P. A.; Vankelecom, I. F. J.; Sels, B. F. CO_2 Reverse Selective Mixed Matrix Membranes for H_2 Purification by Incorporation of Carbon–silica Fillers. *J. Mater. Chem. A* **2013**, *1* (3), 945–953.

(38) Aroon, M. A.; Ismail, A. F.; Matsuura, T.; Montazer-Rahmati, M. M. Performance Studies of Mixed Matrix Membranes for Gas Separation: A Review. *Sep. Purif. Technol.* **2010**, *75* (3), 229–242.

(39) Yu, J.; Wang, C.; Xiang, L.; Xu, Y.; Pan, Y. Enhanced C3H6/C3H8 Separation Performance in Poly(vinyl Acetate) Membrane Blended with ZIF-8 Nanocrystals. *Chem. Eng. Sci.* **2018**, *179*, 1–12.

(40) Vinh-Thang, H.; Kaliaguine, S. Predictive Models for Mixed-Matrix Membrane Performance: A Review. *Chem. Rev.* **2013**, *113* (7), 4980–5028.

(41) Safarpour, M.; Vatanpour, V.; Khataee, A.; Esmaeili, M. Development of a Novel High Flux and Fouling-Resistant Thin Film Composite Nanofiltration Membrane by Embedding Reduced Graphene. *Sep. Purif. Technol.* **2015**, *154*, 96–107.

(42) Kim, E.-S.; Hwang, G.; Gamal El-Din, M.; Liu, Y. Development of Nanosilver and Multi-Walled Carbon Nanotubes Thin-Film Nanocomposite Membrane for Enhanced Water Treatment. *J. Memb. Sci.* **2011**, *394–395* (395), 37–48.

(43) Lind, M. L.; Jeong, B.-H.; Subramani, A.; Huang, X.; Hoek, E. M. V. Effect of Mobile Cation on Zeolite-Polyamide Thin Film Nanocomposite Membranes. *J. Mater. Res.* **2009**, *24* (5), 1624–1631.

(44) Leus, K.; Bogaerts, T.; De Decker, J.; Depauw, H.; Hendrickx, K.; Vrielinck, H.; Van

Speybroeck, V.; Van Der Voort, P. Systematic Study of the Chemical and Hydrothermal Stability of Selected “stable” Metal Organic Frameworks. *Microporous Mesoporous Mater.* **2016**, *226*, 110–116.

(45) Sun, C.-Y.; Qin, C.; Wang, X.-L.; Yang, G.-S.; Shao, K.-Z.; Lan, Y.-Q.; Su, Z.-M.; Huang, P.; Wang, C.-G.; Wang, E.-B. Zeolitic Imidazolate Framework-8 as Efficient pH-Sensitive Drug Delivery Vehicle. *Dalt. Trans.* **2012**, *41* (23), 6906.

(46) Pang, S. H.; Han, C.; Sholl, D. S.; Jones, C. W.; Lively, R. P. Facet-Specific Stability of ZIF-8 in the Presence of Acid Gases Dissolved in Aqueous Solutions. *Chem. Mater.* **2016**, *28* (19), 6960–6967.

(47) Bhattacharyya, S.; Pang, S. H.; Dutzer, M. R.; Lively, R. P.; Walton, K. S.; Sholl, D. S.; Nair, S. Interactions of SO 2 -Containing Acid Gases with ZIF-8: Structural Changes and Mechanistic Investigations. *J. Phys. Chem. C* **2016**, *120* (48), 27221–27229.

(48) Park, K. S.; Ni, Z.; Côté, A. P.; Choi, J. Y.; Huang, R.; Uribe-Romo, F. J.; Chae, H. K.; O’Keeffe, M.; Yaghi, O. M. Exceptional Chemical and Thermal Stability of Zeolitic Imidazolate Frameworks. *Proc. Natl. Acad. Sci. U. S. A.* **2006**, *103* (27), 10186–10191.

(49) Aert, S. Van; Verbeeck, J.; Erni, R.; Bals, S.; Luysberg, M.; Dyck, D. Van; Van Tendeloo, G. Quantitative Atomic Resolution Mapping Using High-Angle Annular Dark Field Scanning Transmission Electron Microscopy. *Ultramicroscopy 109*, 1236–1244.

(50) Tsai, C.-W.; Langner, E. H. G. The Effect of Synthesis Temperature on the Particle Size of Nano-ZIF-8. *Microporous Mesoporous Mater.* **2016**, *221*, 8–13.

(51) Ghosh, S.; Kinthada, L. K.; Bhunia, S.; Bisai, A. Lewis Acid-Catalyzed Friedel–Crafts Alkylations of 3-Hydroxy-2-Oxindole: An Efficient Approach to the Core Structure of Azonazine. *Chem. Commun.* **2012**, *48* (81), 10132.

(52) Fan, X.; Dong, Y.; Su, Y.; Zhao, X.; Li, Y.; Liu, J.; Jiang, Z. Improved Performance of Composite Nanofiltration Membranes by Adding Calcium Chloride in Aqueous Phase during Interfacial Polymerization Process. *J. Memb. Sci.* **2014**, *452*, 90–96.

(53) Tang, C.; Kwon, Y.; Leckie, J. Probing the Nano- and Micro-Scales of Reverse Osmosis membranes—A Comprehensive Characterization of Physiochemical Properties of Uncoated and Coated Membranes by XPS, TEM, ATR-FTIR, and Streaming Potential Measurements. *J. Memb. Sci.* **2007**, *287* (1), 146–156.

(54) Shantarovich, V. P.; Suzuki, T.; He, C.; Gustov, V. W. Inhibition of Positronium Formation by Polar Groups in Polymers—relation with TSL Experiments. *Radiat. Phys. Chem.* **2003**, *67* (1), 15–23.

(55) Fujioka, T.; Oshima, N.; Suzuki, R.; Price, W. E.; Nghiem, L. D. Probing the Internal Structure of Reverse Osmosis Membranes by Positron Annihilation Spectroscopy: Gaining More Insight into the Transport of Water and Small Solutes. *J. Memb. Sci.* **2015**, *486*, 106–118.

(56) Fairen-Jimenez, D.; Moggach, S. A.; Wharmby, M. T.; Wright, P. A.; Parsons, S.; Düren, T. Opening the Gate: Framework Flexibility in ZIF-8 Explored by Experiments and Simulations. *J. Am. Chem. Soc.* **2011**, *133* (23), 8900–8902.

(57) Bushell, A. F.; Attfield, M. P.; Mason, C. R.; Budd, P. M.; Yampolskii, Y.; Starannikova, L.; Rebrov, A.; Bazzarelli, F.; Bernardo, P.; Carolus Jansen, J.; Lanč, M.; Friess, K.; Shantarovich, V.; Gustov, V.; Isaeva, V. Gas Permeation Parameters

of Mixed Matrix Membranes Based on the Polymer of Intrinsic Microporosity PIM-1 and the Zeolitic Imidazolate Framework ZIF-8. *J. Memb. Sci.* **2013**, *427*, 48–62.

(58) Mulder, M. *Basic Principles of Membrane Technology*; Kluwer Academic, 1991.

(59) Thompson, J. A.; Chapman, K. W.; Koros, W. J.; Jones, C. W.; Nair, S. Sonication-Induced Ostwald Ripening of ZIF-8 Nanoparticles and Formation of ZIF-8/polymer Composite Membranes. *Microporous Mesoporous Mater.* **2012**, *158*, 292–299.

Supporting information

The role of MOFs in Thin-Film Nanocomposite (TFN) membranes

Cédric Van Goethem,[a] Rhea Verbeke,[a] Martin Pfanmöller,[b,c] Tönjes Koschine,[a] Marcel Dickmann[e], Werner Egger[d], Sara Bals,[b] Ivo F.J. Vankelecom[a,]*

[a] Center for Surface Chemistry and Catalysis, Faculty of Bioscience Engineering Sciences, KU Leuven, Celestijnenlaan 200F PO Box 2461, 3001 Leuven, Belgium

[b] Electron Microscopy for Material Science (EMAT), Department of Physics, University of Antwerp, Groenenborgerlaan 171, Antwerp 2020 Belgium, Belgium

[c] Centre for Advanced Materials, Heidelberg University, 69120 Heidelberg, Germany

[d] Institut für Angewandte Physik und Messtechnik, Universität der Bundeswehr München, Werner-Heisenberg-Weg 39, 85579 Neubiberg, Germany

[e] FRM II, Technische Universität München, Lichtenbergstraße 1, 85748 Garching, Germany

Corresponding author:

* ivo.vankelecom@kuleuven.be

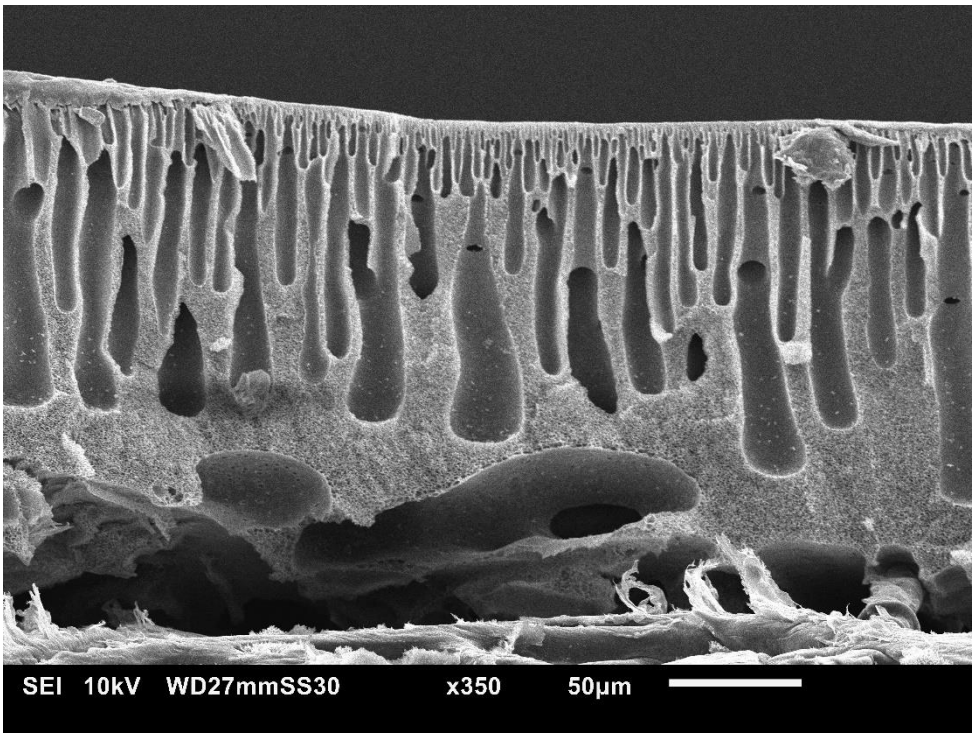

Figure S1. SEM cross-section image showing the macrovoid structure of the support membranes.

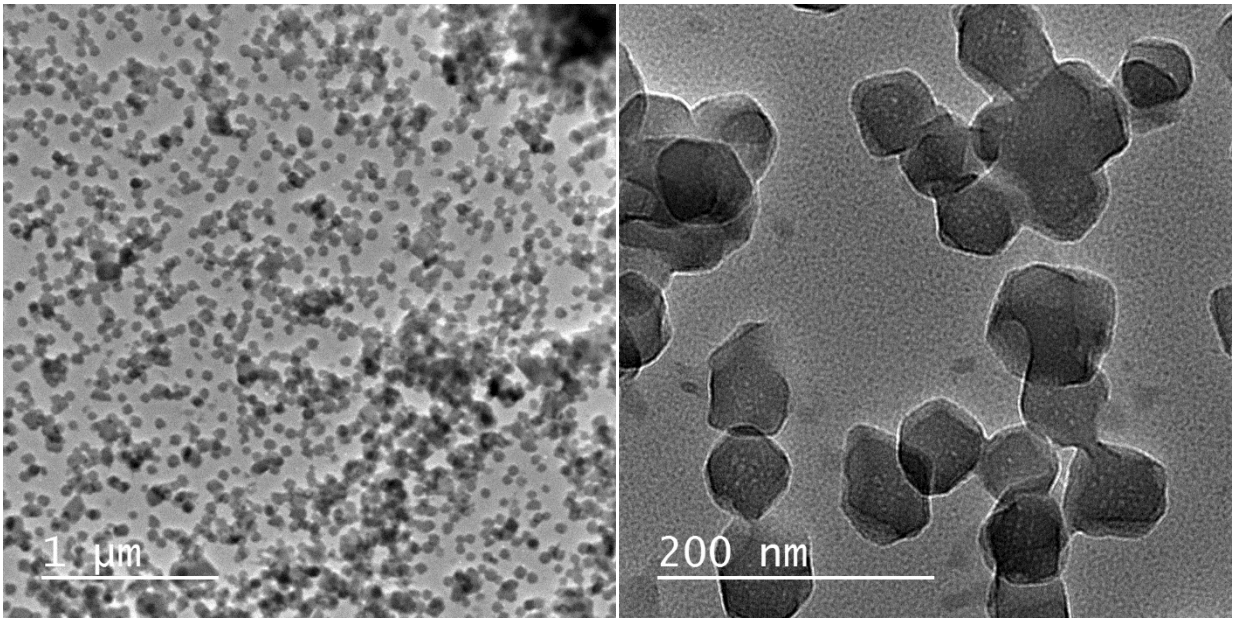

Figure S2. Representative low and high magnification TEM images showing the synthesized ZIF-8 particles. Images were acquired on a Jeol ARM-200F microscope operated at 200 kV. The Hercules fund (project AKUL/13/19) is kindly acknowledged for funding the microscope.

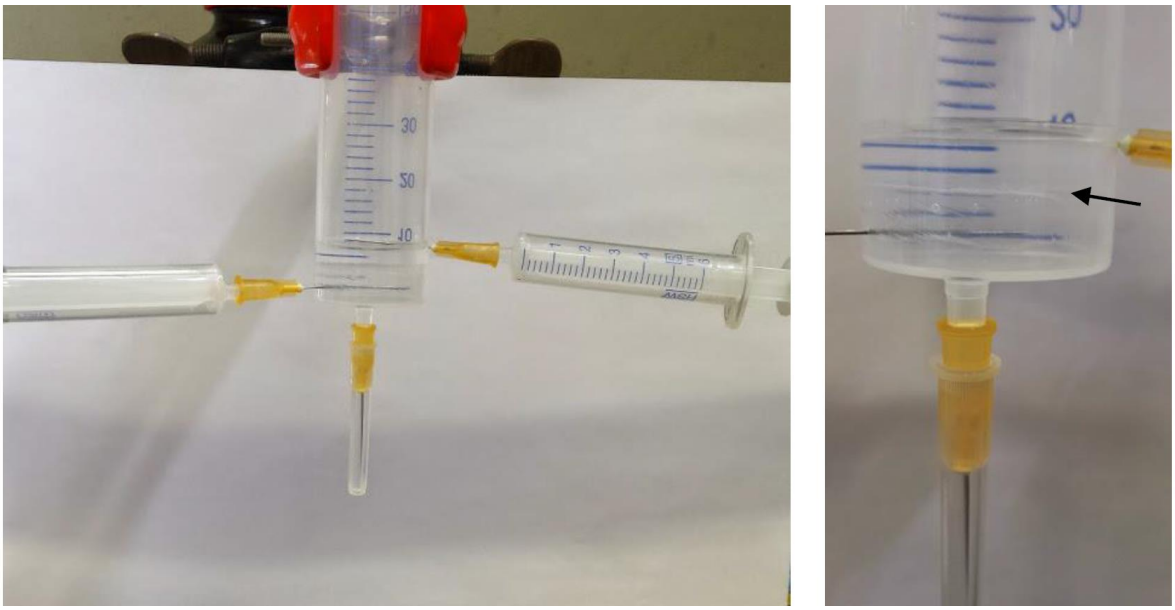

Figure S3. Experimental setup for the preparation of free-standing PA films. The PA film formed at the interface is indicated with a black arrow.

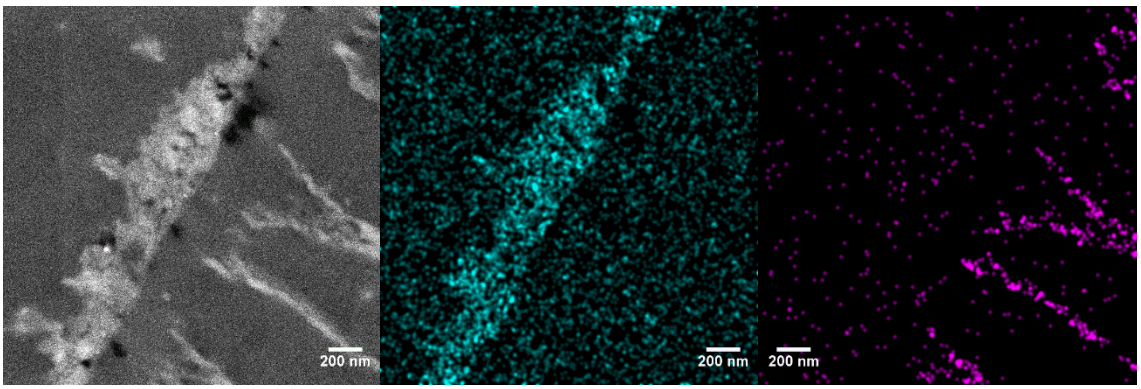

Figure S4. HAADF-STEM image (left), N-map (middle) and S-map (right) of the 0.005 w/v% ZIF-EFP membrane.

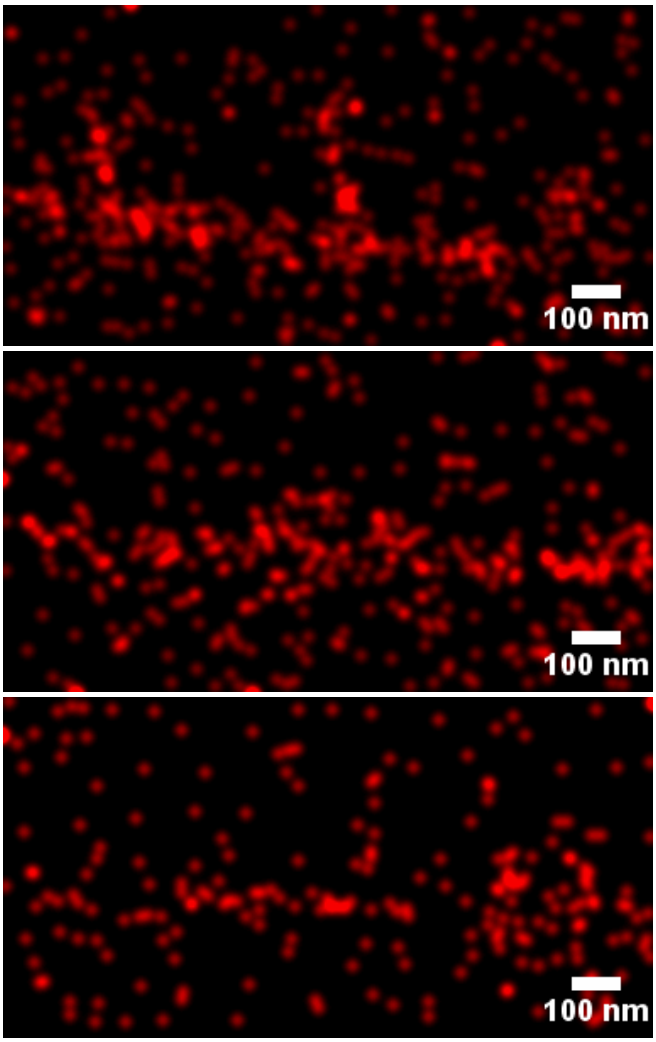

Figure S5. STEM-EDX (cross-section) Zn-mappings taken at different locations along the toplayer of the 0.1 w/v% ZIF-EFP membrane.

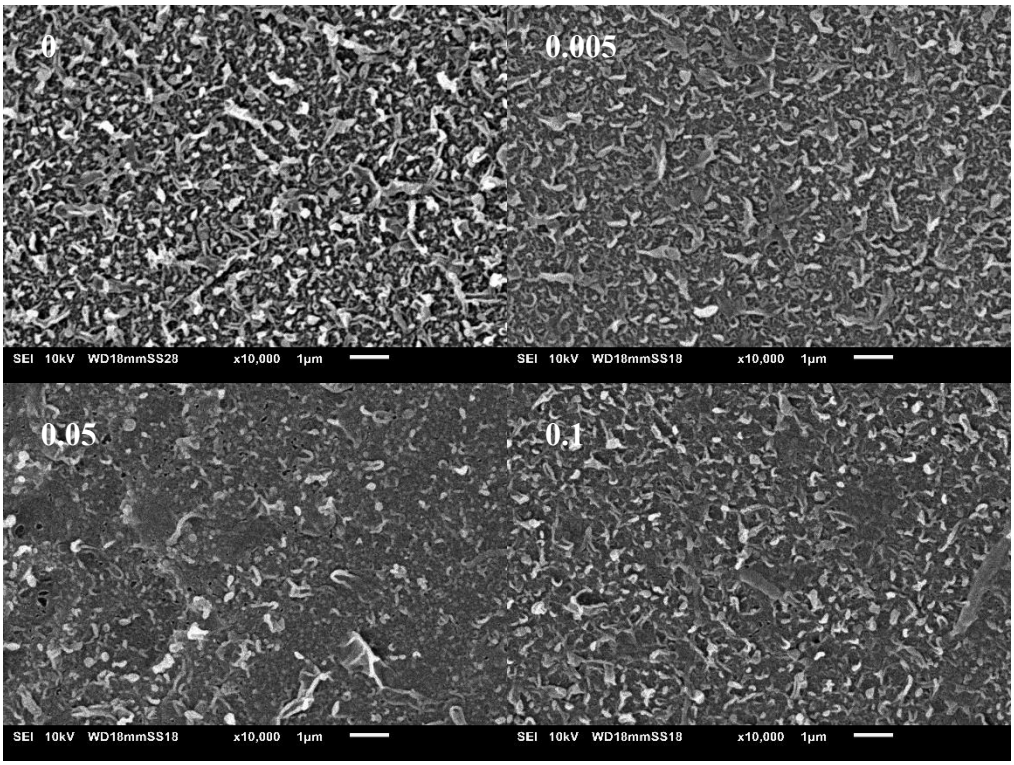

Figure S6. SEM topview images of HMim-TFC membranes. The HMim concentration is indicated on the images.

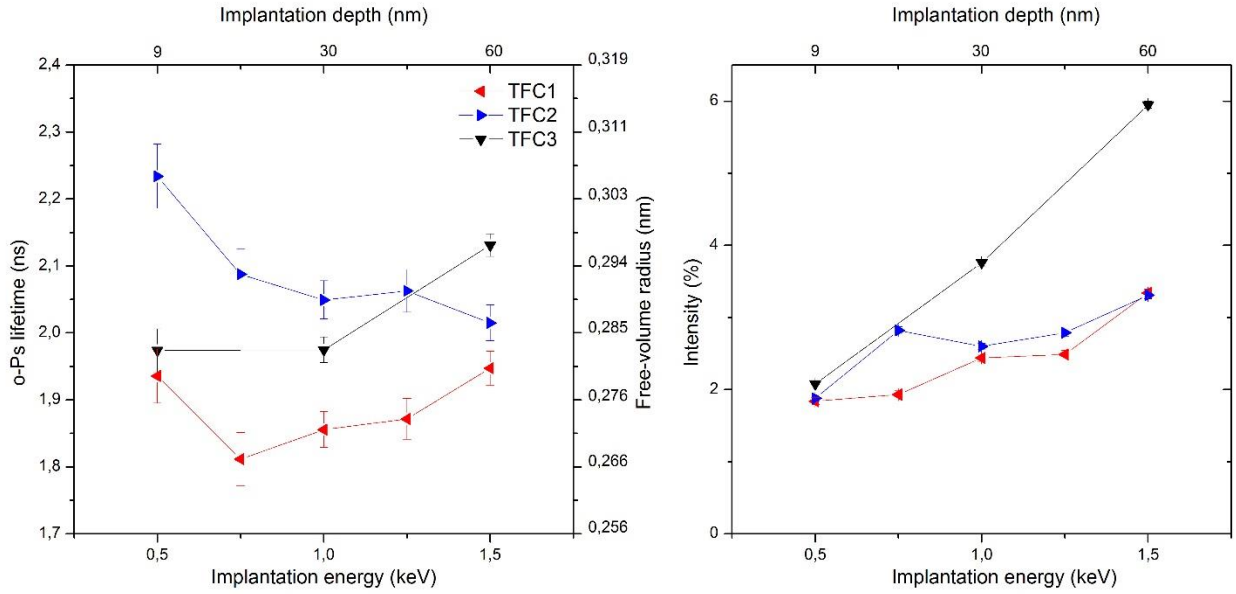

Figure S7. o-Ps lifetime and intensity as function of the positron implantation energy for the reference TFC membrane measured at 3 different spots.

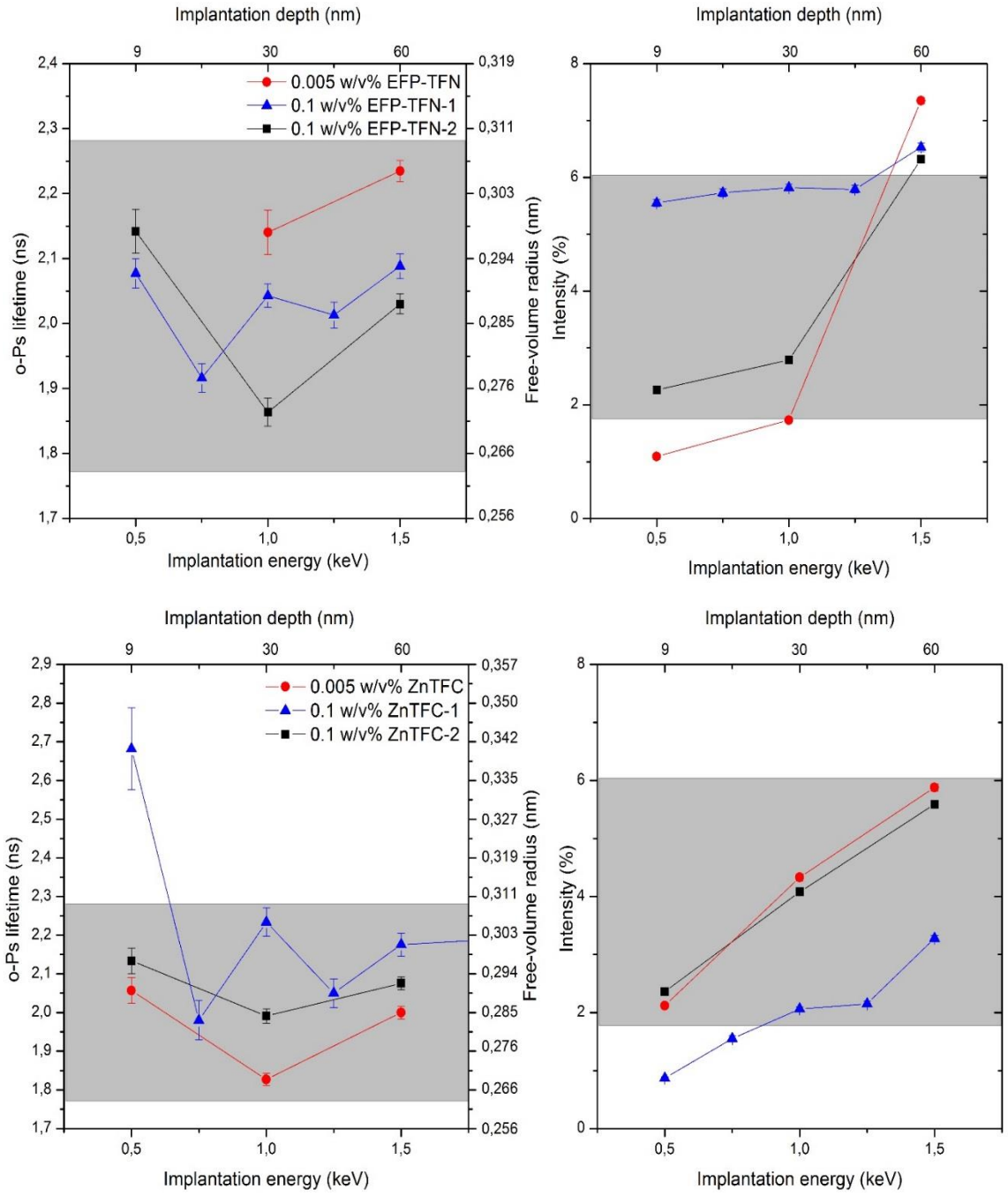
Implantation depth (nm)
9
30
60
0.005 w/v% EFP-TFN
0.1 w/v% EFP-TFN-1
0.1 w/v% EFP-TFN-2
o-Ps lifetime (ns)
Free-volume radius (nm)
Intensity (%)
Implantation energy (keV)
0.005 w/v% ZnTFC
0.1 w/v% ZnTFC-1
0.1 w/v% ZnTFC-2

Figure S8. o-Ps lifetime and intensity as function of the positron implantation energy for (top) EFP and reference TFC membranes and (bottom) Zn-TFC and reference TFC membranes.

Supporting Table 1. XPS-based O/N ratio's for ZIF-8 based TFN membranes prepared according to the Evaporation Controlled filler Positioning (EFP) and traditional (TRAD) membranes. Data taken from[10].

Sample	O/N
sZIF-EFP 0.01 w/v%	1.91
sZIF-EFP 0.2 w/v%	1.68
bZIF-EFP 0.005 w/v%	1.57
bZIF-EFP 0.2 w/v%	2.14
bZIF-TRAD 0.01 w/v%	2.82
bZIF-TRAD 0.1 w/v%	2.16

Supporting table 2. Permeance and rejection values for the Zn-TFC, Mim^{-}-TFC and bZIF-EFP membranes.

Sample	Permeance (l/m².h.bar)	Rejection NaCl (%)	Rejection MO (327 Da, %)
Zn-TFC (0 wt%)	0.505 ± 0.088	77.5 ± 1.7	96.0 ± 3.2
Zn-TFC (0.005 wt%)	0.700 ± 0.081	75.5 ± 3.8	98.8 ± 1.5
Zn-TFC (0.050 wt%)	1.351 ± 0.413	55.0 ± 4.1	96.1 ± 3.8
Zn-TFC (0.100 wt%)	2.157 ± 0.110	59.0 ± 11.1	97.6 ± 4.2
Mim^{-}-TFC (0 wt%)	0.411 ± 0.081	77.5 ± 1.7	n.d.
Mim^{-}-TFC (0.005 wt%)	0.551 ± 0.122	75.5 ± 4.9	n.d.
Mim^{-}-TFC (0.050 wt%)	0.594 ± 0.177	65.4 ± 8.7	n.d.
Mim^{-}-TFC (0.100 wt%)	0.619 ± 0.116	67.8 ± 5.6	n.d.
bZIF-EFP (0 w/v%)[a]	0.946 ± 0.212	86.0 ± 2.9	n.d.
bZIF-EFP (0.005 w/v%)[a]	2.750 ± 0.277	82.3 ± 14.3	n.d.
bZIF-EFP (0.1 w/v%)[a]	1.927 ± 0.356	60.9 ± 14.7	n.d.

[A] C. Van Goethem, R. Verbeke, S. Hermans, R. Bernstein, I.F.J. Vankelecom, Controlled positioning of MOFs in interfacially polymerized thin-film nanocomposites, J. Mater. Chem. A. 4 (2016) 16368–16376. doi:10.1039/C6TA05175H.